Reexamination of the Li^+-He interaction potential

P. P. Ong, M. J. Hogan, and T. L. Tan
Physics Department, National University of Singapore, Kent Ridge Crescent, Singapore 0511, Republic of Singapore
(Received 23 April 1992; revised manuscript received 7 July 1992)

Using various recently proposed interaction potentials for the Li^+-He system, elaborate calculations of the mobility, longitudinal, and transverse diffusion coefficients of Li^+ swarms in helium have been made by high-speed Monte Carlo simulations (MCS's). In addition, the transverse diffusion coefficients for this ion–neutral-atom pair have been experimentally measured with total errors of ±3%. The close agreement of the present experimental results with those of Skullerud, Eide, and Stefansson [J. Phys. D **19**, 197 (1986)] as well as the faithful MCS reproduction of all three transport coefficients using the interaction potential proposed by Larsen *et al.* [J. Phys. B **21**, 2519 (1988)] over the entire range of E/N (electric field to neutral-particle number density ratio) studied not only provides confirmation of their transport coefficient values, but also lends strong support for their proposed interaction potential. In comparison, the more recent potentials of Ahlrichs *et al.* [J. Chem. Phys. **88**, 6290 (1988)] and of Koutselos, Mason, and Viehland [J. Chem. Phys. **93**, 7125 (1990)] did not reproduce the experimental data quite as well. As a benchmark the MCS calculations have also provided evidence of the accuracy of the Kramers-Moyal expansion method in calculating the transport coefficients.

PACS number(s): 34.20.Cf, 51.50.+v, 52.25.Fi

INTRODUCTION

The elastic interaction of atomic particles is of intrinsic importance in understanding the propagation of gaseous matter, heat, sound, and electrical currents in a gaseous medium. Where one of the species is a charged ion, this interaction is particularly pertinent to gaseous electrical conduction and the sustenance of gas plasmas such as those occurring in gas cavity lasers. It fundamentally controls the cross section and momentum transfer at each collision between the species, and, on the macroscopic scale, ultimately determines the transport coefficients of the ions drifting in the neutral medium. Theoretically, a chief goal is to obtain accurate values of the interaction potential and to solve the formidable Boltzmann equation by various approaches so as to reproduce the transport coefficients from an assumed form of interaction potential. Experimentally, only the transport coefficients, and not the interactions at the microscopic level, are directly measurable, and so it is necessary to invert the experimental data to obtain information about the interaction.

In this paper we report results of Monte Carlo simulation (MCS) calculations of the transport coefficients of Li^+ in He and experimental measurements of D_T/K, the ratio of the transverse diffusion coefficient to mobility, of the same ion–neutral-atom pair. With only four electrons, the Li^+-He ($X\,^1\Sigma^+$) electronic configuration is the simplest spherically symmetric singlet-ground-state system that may be studied both theoretically and experimentally. Unfortunately, partly because of its simplicity, there arises an embarrassment and some confusion of too many proposed interaction potentials without even the most recent ones agreeing entirely. For this reason, it is hoped that the present reexamination will help to resolve conclusively the discrepancies and single out the most reliable interaction potential.

BRIEF SURVEY OF EXISTING POTENTIALS

The long-range induced-dipole-polarization potential for the Li^+-He system is well established and is given (in atomic units) by

$$V(r) = -\alpha/2r^4 , \tag{1}$$

where the polarizability $\alpha = 1.3831$. However, in the short and intermediate ranges there are still some discrepancies among the various interaction potentials that have been proposed. In swarm experiments, this region corresponds to the intermediate- to high-(E/N) range and straddles both sides of the potential minimum.

Following the pioneering *ab initio* self-consistent-field (SCF) calculations of the potential-energy curves of Li^+-He by Catlow *et al.* [1], Hariharan and Staemmler [2] introduced the correlated electron-pair approximation (CEPA) of the united-atom model and obtained a significantly deeper potential well. Using totally different approaches, Waldman and Gordon [3] applied scaling of their semiempirical electron-gas Drude harmonic-oscillator model (EGDM), while Polak-Dingels *et al.* [4] conducted low-energy beam-scattering experiments of Li^+ by He and deduced a Morse–spline–van der Waals synthesized potential curve that is expected to be more accurate in the repulsive region. Gatland *et al.* [5] inverted their mobility data of Li^+ drifting in He and deduced a set of directly determined potentials. Senff and Burton [6] extended the CEPA calculations using the same supermolecule approach, but with a much larger Gaussian basis set, and obtained an even deeper potential well. Ahlrichs *et al.* [7] simplified the short-range contributions by lumping the short-range dispersive terms with the SCF repulsive term to yield an effective SCF term. Over a three-year period, Skullerud and his co-workers [8–10] made measurements of all the primary transport

coefficients of Li^+ in He, and using the Kramers-Moyal expansion of the Boltzmann collision integral to invert their data, deduced a tabulated set of the interaction potential, which could reproduce the measured transport coefficients. Most recently, Koutselos *et al.* [11] assumed a double-exponential function for the short-range potential whose parameters may be set by a universal scaling rule, and derived general formulas for the interaction potentials of closed-shell atoms and ions. Values of the transport coefficients obtained from recent MCS calculations using this potential have proven to agree fairly well with experimental data for various interactions of potassium and sodium ions with helium, neon, argon, and krypton atoms [12–16].

Table I summarizes the resulting values, in atomic units, obtained from the above works, of r_0, the position where $V(r)=0$; r_m, the minimum of $V(r)$; and $|V(r_m)|$, the depth of the potential well, that characterize the potential-energy curve in the short to intermediate range. In most cases, r_0 is not explicitly given in the publications and is extracted by interpolation from the data points available.

The last four potentials, referred to, respectively, as the Senff and Burton (SB) potential, the Larsen, Skullerud, Lovaas, and Stefansson (LSLS) potential, the modified Tang-Toennies (MTT) potential of Ahlrichs *et al.*, and the Koutselos, Mason, and Viehland (KMV) potential, were selected for detailed testing using the MCS technique described below. For the two analytic potentials (MTT and KMV), the following formulas were used:

$$V_{\mathrm{KMV}}(r)=V_0[A_1\exp(-a_1r/\rho)-B_1\exp(-b_1r/\rho)] -F[C_4/r^4+(C_{6\mathrm{ind}}+C_{6\mathrm{disp}})/r^6 +(C_{8\mathrm{ind}}+C_{8\mathrm{disp}})/r^8] \quad (2)$$

with

$$F=\begin{cases}1 & \text{for } r>1.28r_m\ ,\\ \exp[-(1.28r_m/r-1)^2] & \text{otherwise}\ ,\end{cases} \quad (3)$$

where the subscripts "ind" and "disp" represent, respectively, the inductive and dispersive hyperpolarizability coefficients and where, for Li^+ in He, in atomic units, $V_0=0.1135$, $A_1=146.98$, $a_1=1.5024$, $B_1=70.198$, $b_1=1.4041$, $\rho=0.7185$, $C_4=0.6916$, $C_{6\mathrm{ind}}=1.2217$, $C_{6\mathrm{disp}}=0.2962$, $C_{8\mathrm{ind}}=5.307$, $C_{8\mathrm{disp}}=2.044$, and $r_m=3.64$, and

$$V_{\mathrm{MTT}}(r)=1.31A_1\exp(-b_1r)-F_4-F_6-F_8-F_{10}\ , \quad (4)$$

where

$$F_p=D_p\left[1-\exp(-b_1r)\sum_{j=0}^{p}[(b_1r)^j/j!]\right]r^{-p} \quad (5)$$

with

$$D_4=\tfrac{1}{2}\alpha_1,\quad D_6=\tfrac{1}{2}\alpha_2+C_6\ ,\quad D_8=\tfrac{1}{2}\alpha_3+C_8,\quad D_{10}=\tfrac{1}{2}\alpha_4+C_{10}\ . \quad (6)$$

For Li^+ in He, $A_1=23.92$, $b_1=2.694$, $\alpha_1=1.38$, $\alpha_2=2.44$, $\alpha_3=10.60$, $\alpha_4=80.00$, $C_6=0.298$, $C_8=1.97$, and $C_{10}=18.80$.

For the two potentials (SB and LSLS) that are available in pointwise form only, a clamped-cubic-spline fit is used to interpolate for $V(r)$ at intermediate values of r not given in the table. The end spline at the short-range end is clamped to yield the same curvature as the Born-Mayer exponential decay curve fitting the two extreme data points. The same curve is then used to extrapolate for all $V(r)$ at points beyond the smallest available r in the table. A similar scheme is used for the far-end spline, which is clamped to give the same curvature as that obtained from Eq. (1).

A plot of the four different potentials including the interpolated cubic-spline curves linking successive data points for the last two potentials are shown in Fig. 1. The respective potentials are represented on a linear scale for $V(r)<0.005E_h$ ($E_h=1$ hartree), and on a logarithmic scale for $V(r)$ above this value. Note that all the potentials agree well only in the long-range limit. The significant variations in their attractive wells and repulsive walls will be of greater interest here.

THE MONTE CARLO SIMULATION METHOD

Except for the simplest cases, the Boltzmann equation arising from a calculation of the transport coefficients from a given interaction potential can hitherto only be solved by numerical iterative methods which unfortunately suffer occasionally from less-than-realistic simplifications as well as from nonconvergence of the answers pursued. The alternative MCS approach employed here overcomes both the above problems by relying largely on the speed and power of a modern supercomputer. Details of our MCS procedure have been pre-

TABLE I. Comparison of the vital parameters characterizing the Li^+-He interaction potential (in a.u.).

Reference	Authors	Method	r_0	r_m	$V(r_m)$
[1]	Catlow *et al.*	SCF	3.02	3.72	−0.0025
[2]	Hariharan and Staemmler	CEPA	3.02	3.63	−0.002 74
[5]	Gatland *et al.*	mobility inversion	3.04	3.70	−0.002 72
[3]	Waldman and Gordon	scaled EGDM	3.06	3.17	−0.0025
[4]	Polak-Dingels *et al.*	beam scattering	3.08	3.70	−0.0026
[6]	Senff and Burton	extended CEPA	2.97	3.58	−0.002 955
[10]	Larsen *et al.*	mobility modified	2.95	3.54	−0.003 01
[7]	Ahlrichs *et al.*	effective SCF	2.99	3.57	−0.00 286
[11]	Koutselos *et al.*	short-range scaling	3.01	3.64	−0.00 270

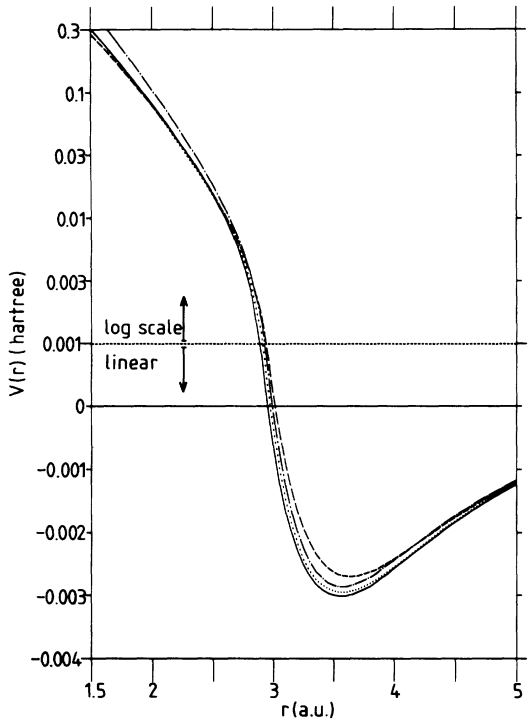

FIG. 1. Various proposed interaction potentials for the Li^+-He system. A dashed line represents the KMV potential, a dashed-dotted line the MTT potential, a solid line the LSLS potential, and a dotted line the SB potential, the last two being derived by cubic-spline fitting of reported data points.

viously reported [12–16], and because of its proven performance, no modification of the established algorithm is required.

Briefly, the method begins by assuming a realistic input interaction potential $V(r)$ between the ion and the gas particle. The neutral gas is assigned a Maxwellian distribution of velocities at a specific temperature, which in the present case is set to 310 K. From each of the assumed potential inputs described in the preceding section, a table of scattering angles $\chi(\varepsilon,b)$ in the center-of-mass system for 120 geometrically spaced values of center-of-mass collision energy ε, and 200 arithmetically spaced values of impact parameters b, is computed. In the range probed, the atomic masses of the colliding particles are large enough for classical mechanics to yield a sufficiently accurate approximation. It has previously been established [5,10] that a full quantum-mechanical calculation, while entailing huge oscillations in the cross section and vastly increased computation times, introduces, at most, a variation of 0.15% in the mobility values. The ε values cover six decades, while the b values range from zero to a maximum determined, for each ε value, by an arbitrary cutoff small-angle deflection set to $\chi_m = 0.05$ rad. Variations of χ_m from 0.02 to 0.10 rad. did not produce any noticeable difference in the results, except at E/N values below 2 Td, which are outside the range investigated. Also computed are the respective mean free collision frequencies ν at various energies, as the variation of $\nu(\varepsilon)$ with ε is taken into account in determining the probability of the following collision.

The computed values are then employed in a stochastic determination of collision events and their resulting trajectories. In the ensuing bulk simulation, the life history of a single ion is followed over 100 000 collisions. The statistics gathered over 25 such runs are then analyzed to extract the time-averaged values of the three transport coefficients and their associated standard errors. The mobility data are calculated by direct tracking of the ion velocity, and, for the number of collisions sampled, it is quite easy to achieve an accuracy of 0.5%. On the other hand, the diffusion coefficients are calculated from the Kubo relationship [17]

$$D_{T,L} = \lim_{t' \to \infty} \langle v_{T,L}(t) r_{T,L}(t,t') \rangle \ , \tag{7}$$

where $v_{T,L}(t)$ is the appropriate (transverse or longitudinal) *random* velocity of the ion at time t, and $r_{T,L}(t,t')$ its corresponding *random* position at time $(t+t')$ *relative* to that at time t. Its ultimate accuracy therefore depends on the speed of convergence of Eq. (7) as $t' \to \infty$. Where the convergence is slow, t' is necessarily large and the statistical scatter of the data grows accordingly. Thus, because of this convergence dependence, the accuracy of diffusion data is typically only about 1.5–2%. In difficult cases around their peak values the error may become as high as 4% for the worst case. In such difficult cases, the statistics is improved by rerunning the entire program several times using different initial random-number seeds.

The calculations were performed on an NEC model SX1A supercomputer, with each data point requiring, on average, the random-number generator subroutine to be called about 3×10^7 times per run. Because of the large volume of simulation calculations required, even with the present state-of-the-art supercomputer, it is, in practice, only possible to repeat the calculations for a limited number of input interaction potentials.

Table II gives the results of the MCS calculations. These results are also shown graphically in Figs. 2–4 as plots of the reduced mobility K_0, of the transverse diffusion coefficients, and of the longitudinal diffusion coefficient, respectively. The diffusion coefficients are expressed as reduced (transverse, longitudinal) diffusion coefficient-to-mobility ratios defined in an earlier paper and for the reasons stated therein [16]. Again, to remove the temperature dependence of mobility, the mobilities are plotted against the effective temperature [18], as it has been established that to a first approximation T_{eff} yields an equivalent combined effect of the temperature and E/N on mobility on a single scale.

MEASUREMENTS OF D_T/K

Details of the apparatus used to measure D_T/K for K^+- and Na^+-ion swarms in several rare gases have been previously reported [19,20]. Briefly, the method consists of allowing a low-density slit source to introduce ions at one end of a drift tube pressurized with a selected neutral gas. The ions then drift and diffuse under a steady electric field to the other end. The ionic energy parameter, E/N, is rigorously controlled and its value is always

selected to ensure that no ion escapes by the sides of the drift tube so that all ions are eventually accounted for at the opposite end. Under this condition the radial boundary condition of the swarm motion may be approximated to that of an infinite medium. The spatial profile of the ion-current density at the tail end of the drift tube is deduced from the partial currents collected at each of the 33 (reduced from 65 previously) equally spaced linear electrodes arranged parallel to the source slit and in a plane perpendicular to the drift axis. Only data that yield

TABLE II. MCS calculated values of K_0, D_T/K, and D_L/K using (a) the SB potential, (b) the LSLS potential, (c) the MTT potential, and (d) the KMV potential.

E/N (Td)	T_{eff} (K)	K_0 ($cm^2/V\,s$)	D_T/K (mV)	D_L/K (mV)
		(a) SB potential		
5	326	23.40	27.6	29.0
10	377	24.09	30.9	40.4
15	481	25.64	40.2	69.2
20	664	27.63	53.8	111.4
25	954	29.82	75.6	163.5
30	1333	31.32	101.8	207.9
35	1781	32.20	127.9	247.3
40	2284	32.64	162.4	281.7
45	2826	32.75	193.8	321.0
50	3391	32.62	230.3	342.6
55	3969	32.32	269.8	375.2
60	4599	32.07	308.3	412.2
65	5197	31.60	338.0	440.2
70	5839	31.21	377.4	476.5
80	7166	30.41	465.5	567.5
90	8598	29.72	567.7	635.6
100	10 180	29.19	658.9	789.2
120	13 387	28.00	857.1	1023.9
140	16 873	27.01	1109.0	1279.5
160	20 907	26.36	1357.9	1602.4
180	25 137	25.72	1668.2	2042.0
200	29 898	25.27	2010.1	2562.5
		(b) LSLS potential		
2	312	21.87	27.8	28.2
3	315	22.27	28.2	28.2
5	314	22.69	28.0	29.8
10	375	23.76	31.5	39.8
15	478	25.39	39.3	68.4
20	660	27.50	53.4	114.6
25	947	29.66	74.9	168.4
30	1324	31.18	101.9	207.8
35	1765	32.03	128.0	242.2
40	2261	32.45	160.6	277.3
45	2793	32.53	191.9	317.8
50	3357	32.44	231.6	341.6
55	3924	32.12	265.0	371.6
60	4536	31.83	294.8	399.7
65	5130	31.38	342.7	441.7
70	5785	31.06	375.6	476.0
80	7096	30.26	464.5	557.2
90	8524	29.59	554.2	640.1
100	9992	28.91	638.7	754.9
110	11 568	28.34	754.1	902.6
120	13 211	27.81	854.2	999.3
125	14 029	27.53	913.8	1058.3
140	16 724	26.89	1064.2	1289.0
150	18 625	26.51	1215.3	1420.6
160	20 471	26.07	1370.0	1615.7
175	23 670	25.66	1573.4	1922.1
180	24 791	25.54	1640.0	2001.8
200	29 452	25.08	2007.4	2500.6
		(c) MTT potential		
5	326	23.46	27.9	30.5
10	380	24.60	31.5	42.1
15	491	26.36	39.9	69.3
20	681	28.30	53.8	114.8
25	974	30.29	76.0	163.1
30	1344	31.49	100.5	200.6
35	1773	32.11	129.7	232.6
40	2236	32.24	158.5	263.3
45	2739	32.18	187.2	283.9
50	3266	31.95	220.7	327.3
55	3796	31.54	251.9	336.6
60	4359	31.16	288.0	385.5
65	4926	30.71	325.7	395.4
70	5531	30.33	355.5	438.5
80	6701	29.36	436.1	485.4
90	7990	28.61	514.8	578.5
100	9301	27.86	589.3	659.3
120	12 157	26.65	778.1	847.3
140	15 166	25.58	961.1	1052.3
160	18 446	24.73	1153.5	1291.5
180	21 946	24.01	1405.7	1546.9
200	25 573	23.35	1668.5	1841.4
		(d) KMV potential		
5	327	24.58	27.5	29.2
10	384	25.34	31.7	42.1
15	499	26.96	41.6	70.5
20	710	29.37	56.6	115.5
25	1018	31.27	79.6	164.5
30	1413	32.53	106.8	203.4
35	1879	33.25	135.4	245.9
40	2374	33.37	163.6	273.9
45	2910	33.29	202.3	299.7
50	3464	33.00	235.1	323.2
55	4036	32.61	269.2	359.5
60	4640	32.23	301.9	395.0
65	5252	31.78	346.4	429.8
70	5892	31.36	384.4	471.6
75	6543	30.93	423.5	507.0
80	7234	30.56	467.3	578.1
90	8659	29.83	558.7	661.8
100	10 176	29.19	654.9	792.7
110	11 743	28.56	769.2	898.1
120	13 369	27.98	873.3	1023.3
140	17 021	27.13	1122.2	1359.5
160	21 072	26.46	1415.5	1710.3
180	25 622	25.97	1745.1	2222.6
200	30 628	25.58	2064.7	2787.2

results independent of the drift distance, gas pressure, and ion-injection current are accepted. The independence on the drift distance and gas pressure ensures that there was no significant end-effect on the ion profile due to the presence of the collector system. The independence on the ion current ensures that ion space-charge effects on the ion diffusion are negligible. All surfaces exposed to the ions inside the drift tube are gold-plated to minimize contact potentials. The advantages of our fixed-geometry ion-current collection system have previously been highlighted [20].

The same apparatus was used here to measure D_T/K of Li^+ ions in He, except that a commercial thermionic isotopically pure $^7Li^+$ source was employed. No $^6Li^+$ was detectable with the quadrupole mass spectrometer located behind the drift tube. However, it should be pointed out that during the initial burn-in the source produced fairly large quantities of the impurity Na^+ and K^+ ions. These were believed to originate from residual impurities of Na and K compounds present in the thermonic material. In spite of whatever species purification that the lithium material had undergone, the commercial preparation process proved to be still inadequate. A similar experience had earlier been reported by Polak-Dingels *et al.* [4] in their commercial $^6Li^+$ source. It was obvious that the high natural abundance and lower ionization potentials of Na (5.139 V) and K (4.341 V) had strongly enhanced their initial ion production relative to those of Li (5.392 V). Fortunately, the same impurity-ion currents dropped rapidly with time because of faster evaporation, and, after about 1 week of continuous burn-in, the impurity level dropped to a negligible level. This experience reaffirmed our belief that an ion identifier such as the quadrupole mass spectrometer is an essential part of the apparatus, without which one cannot ascertain or monitor the purity level of the ions studied [21].

The experimental results covering the E/N range from 8 to 140 Td and to an estimated total error of $\pm 3\%$ are presented in Table III and included in Fig. 3. The range of drift-tube gas temperatures was 307.7–313.2 K, although most data were collected within 310 ± 1 K. Data were recorded over the pressure range 20.0–50.0 Pa to ascertain their independence of pressure. However, the data presented here were recorded at a pressure in the range 26.7–50.0 Pa. The lower limit of E/N was set by the inability to inject the ions into the drift tube at the appropriate energy without raising the pressure to a value so high that the spatial ion distribution becomes too narrow for accurate curve fitting. The upper limit of E/N was set partly by the geometry of the drift tube and partly by electrical breakdown occurring when the drift tube voltage exceeds a certain limit.

The results are consistent with those of Skullerud *et al.* [8] within the combined error bounds.

DISCUSSION

A first impression of the four interaction potentials plotted in Fig. 1 is that their differences are marginal since some of the curves shown even overlap at several places. However, it will be demonstrated that these differences show up clearly in our transport coefficient calculations.

The relevant reduced mobilities are plotted in Fig. 2. The experimental data of Lovaas *et al.* [9] agree so well with the Kramers-Moyal (KM) calculations [10] that the latter may also be represented by the same curve. They

TABLE III. Currently measured values of D_T/K for Li^+ in He with their associated standard deviations and reduced transverse diffusion-coefficient–to–mobility ratios. The D_T/K values have been adjusted to 310 K [19].

E/N	Average D_T/K	Standard deviation		
(Td)	(mV)	(mV)	(%)	$D_T^{(r)}$
8	28.28	0.68	2.40	0.973
10	31.29	0.37	1.18	1.030
12	32.67	0.41	1.24	1.021
15	39.36	1.89	4.81	1.126
20	55.24	1.32	2.39	1.335
25	75.33	2.04	2.71	1.518
30	102.80	1.15	1.12	1.721
35	130.55	2.34	1.80	1.822
40	161.62	3.48	2.15	1.893
45	193.08	2.31	1.19	1.912
50	226.24	2.68	1.18	1.911
60	301.49	6.39	2.12	1.899
70	386.73	3.73	0.96	1.874
80	471.00	18.84	4.00	1.802
90	549.04	10.31	1.88	1.696
100	649.02	7.51	1.16	1.650
120	854.52	11.92	1.40	1.540
140	1091.47	10.38	0.95	1.464

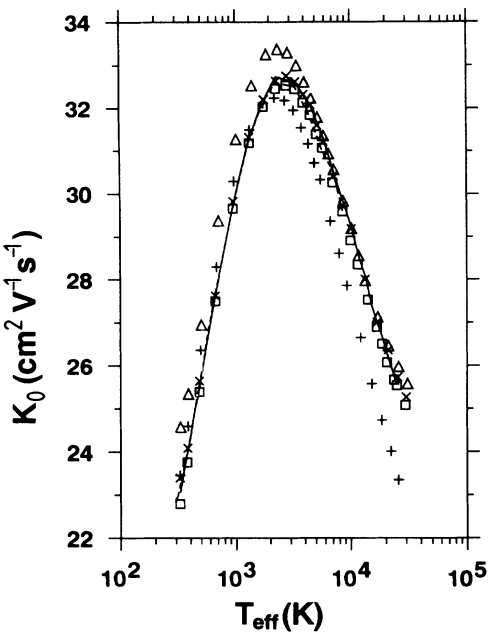

FIG. 2. Reduced mobilities of Li^+ in He obtained by various ways plotted against T_{eff}. Triangles, pluses, crosses, and squares represent the MCS-calculated values using, respectively, the KMV, MTT, SB, and LSLS potentials. Dashed and solid lines represent, respectively, the experimental mobility values of Cassidy and Elford [20] and of Lovaas *et al.* [9].

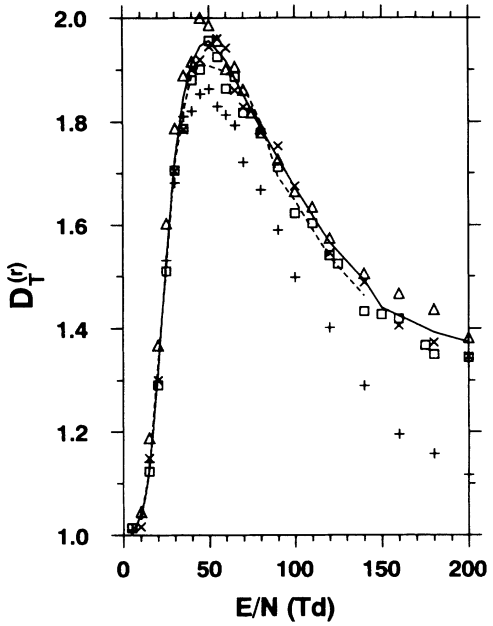

FIG. 3. Reduced transverse diffusion-coefficient–to–mobility ratios of Li^+ in He obtained by various ways plotted against E/N. Triangles, pluses, crosses, and squares represent the MCS-calculated values using, respectively, the KMV, MTT, SB, and LSLS potentials. Dashed and solid lines represent, respectively, the present experimental data and those of Skullerud *et al.* [8].

also agree equally well with the earlier data of Cassidy and Elford [22], except around and above the mobility-peak region where the latter values are up to 1% lower. Curiously, however, the MCS-LSLS results agree almost perfectly with the Cassidy and Elford data throughout the entire range of the latter, although the LSLS potential was derived from the data of Skullerud *et al.*

At low E/N, the MCS-calculated values using the LSLS and SB potentials agree very well with the experimental data, while those obtained from the KMV and MTT potentials deviate considerably from these data. Since all the interaction potentials have the same long-range induced-dipole-polarization interaction given in Eq. (1), the deviation may be attributed only to the difference in the depth of the potential well, and, to a lesser extent, its position and width. For low collision energies ε, these parameters dominate the determination of the integral in the scattering-angle formula. As a guide, the potential well is so shallow that its position and width do not vary much with the different potentials. The difference in the calculated mobilities at low E/N is hence due mainly to the difference in the depth of the potential well. A larger well depth produces a greater scattering angle and thence a larger cross section and a correspondingly smaller mobility. This explanation is consistent with the fact that the KMV potential well depth, being the shallowest, yields the largest mobility. The MTT potential well is slightly shallower than that of the SB or LSLS potential and accordingly yields a slightly larger mobility.

As T_{eff} increases, the mobility rises until it reaches a peak corresponding to $E/N \approx 40$ Td or $T_{eff} \approx 2500$ K. This peak occurs when the two collidants spend a relatively longer time around an interatomic separation where the repulsive term of $V(r)$ is roughly cancelled by the attractive terms, and the target neutral particles appear fairly transparent. Their resistance to the ionic motion is small and so the ionic mobility exhibits a peak. The small differences of r_0 for all the four potentials explains why all the mobility peaks occur at around the same T_{eff}. The heights of the peaks, however, vary considerably. The MCS-SB and MCS-LSLS data agree well with the experimental data, but the MCS-KMV data are significantly much higher while the MCS-MTT data are lower.

As T_{eff} increases beyond the mobility-peak region, the collision energies progressively become larger than the potential well depth, whose significance diminishes rapidly until it has a negligible effect, and so the collisions probe mainly the repulsive potential wall. The continued good agreement between the experimental and MCS mobilities derived from the SB and LSLS potentials suggests that these potentials represent the potential wall fairly well too. The KMV-derived mobilities decrease relatively less rapidly from the peak, thus suggesting that the slope of the KMV potential wall is too soft. In contrast, the MTT-derived mobilities are too low, demonstrating that the repulsive MTT potential slope is too hard. Lacking a double-exponential function, the short-range MTT parameters could not be finely tuned to fit the experimental potentials.

The transverse and longitudinal diffusion plots depict-

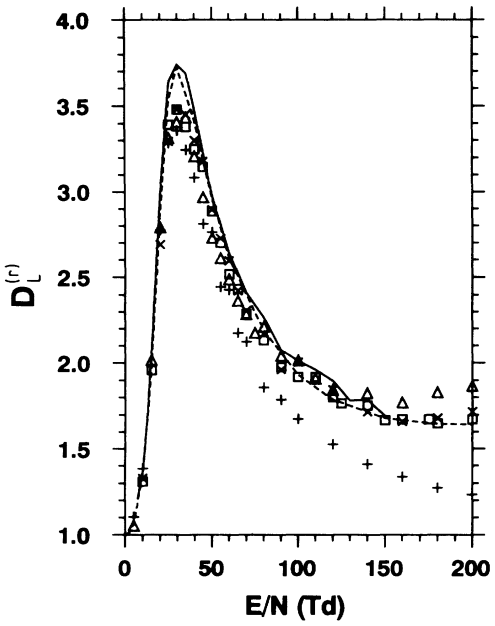

FIG. 4. Reduced longitudinal diffusion-coefficient–to–mobility ratios of Li^+ in He obtained by various ways plotted against E/N. Triangles, pluses, crosses, and squares represent the MCS-calculated values using, respectively, the KMV, MTT, SB, and LSLS potentials. A solid line represents the experimental data of Lovaas *et al.* [9]. A dashed line represents the values calculated using the Kramers-Moyal method [10].

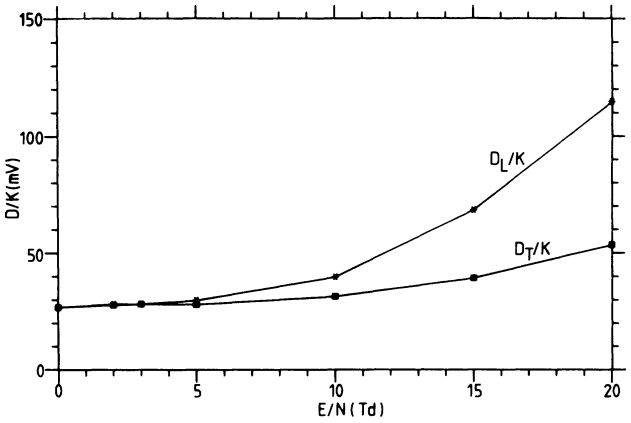

FIG. 5. Plots against E/N of the MCS-calculated D_T/K and D_L/K data using the LSLS potential; showing their expected zero-field limit of 26.7 mV at 310 K.

ed, respectively, in Figs. 3 and 4 show similar results of the MCS calculations for the respective interaction potentials. The KM results for $D_T^{(r)}$ are not shown in Fig. 3 because they agree very well with the experimental data of Skullerud *et al.* In comparison with the mobility plots, by virtue of the higher-power dependence of the reduced diffusion coefficient-to-mobility ratios on E/N, the diffusion plots are less sensitive at the low-(E/N) region and more so at the higher-(E/N) range. This variation of E/N dependence is consistently observed in Figs. 3 and 4.

At low E/N all the potentials yield close agreement of both $D_T^{(r)}$ and $D_L^{(r)}$. As a further demonstration of their accuracy, a plot of D_T/K and D_L/K against E/N, as E/N tends towards zero, is made in Fig. 5 for the LSLS potential, which is typically representative of the rest. As shown on the graph, both D_T/K and D_L/K approach the theoretical limit of 26.7 mV based on the Einstein equation,

$$D_{T,L}/K = kT/e \ , \tag{8}$$

with $T=310$ K. Theoretically, for very low E/N, both D_T and D_L vary as $(E/N)^2$ and their plots against $(E/N)^2$ should be a straight line. However, for the case of Li^+ drifting in He, the onset of the deviation from the $(E/N)^2$ variation of the diffusion coefficients occur at E/N values lower than those obtained here.

At high E/N, the discrepancies arising from the differences in potential shown in Figs. 3 and 4 are magnified in comparison to those of Fig. 2. The calculations reveal a large downward diversion of the MTT-derived diffusion coefficients, and a lesser upward diversion of the KMV-derived diffusion coefficients in comparison with the rest. On the other hand, the same magnification effect produces little increase in the discrepancy of the SB- and LSLS-derived values with the experimental data.

At intermediate E/N, the longitudinal diffusion peaks at around 30 Td, in contrast to the peak at around 45 Td for the transverse diffusion. This shift in peak is because, apart from the energy associated with the ion random motion, the former coefficient involves an additional collision energy attributed to the forward ion drift velocity, which is absent from the latter case. Around each peak, the MCS calculations are relatively less accurate because of slower convergence as a function of MCS sampling time. This is understandable since each peak corresponds to the region at which the gas particles appear most transparent to the ion, and hence a longer sampling time is needed. However, increasing the sampling time would result in a greater statistical spread, and hence a greater standard error, in the sampling.

Since both the MCS and the Kramers-Moyal (KM) calculations using the *same* input LSLS potential, but completely different approaches, agree well with the same set of experimental data for all three transport coefficients, the present MCS calculations provide direct indication of the degree of accuracy of the KM expansion method. At both low and high E/N, the KM method is almost exact, while at intermediate to high E/N it tends to yield only very slightly higher values of all the transport coefficients.

CONCLUSIONS

Our elaborate MCS calculations have revealed that the LSLS and SB potentials are decidedly better representations of the Li^+-He potential than the MTT and KMV potentials. Gratifyingly, the mobility calculations could

even discern very slight differences in the SB and LSLS potentials, thus strongly demonstrating the effectiveness, sensitivity, and accuracy of these calculations. The loss in flexibility of the pointwise potentials of LSLS and SB in comparison with the analytic forms of the KMV and MTT potentials has been effectively compensated by constructing a cubic-spline-fitting curve for each of the intermediate segments of r between two successive data points.

The present study has conclusively established the interaction potential of the simplest alkali-metal-ion–rare-gas system to a new level of accuracy. It is hoped that it will set the pace for similar standards of accuracy for other alkali-metal-ion–rare-gas pairs. As a second benefit, the MCS calculations have also endorsed the accuracy of the Kramers-Moyal expansion method by obtaining almost identical transport coefficients using a completely different approach.

With the ever-increasing power of the supercomputer, we should soon be able to increase further the volume and, hence, the accuracy of the diffusion-coefficient calculations to match those for the mobility coefficients. Attaining this would afford us an even more sensitive test—based on diffusion-coefficient values—to probe more accurately the high-(E/N) and the more unsettled repulsive regions of the intermolecular interaction potential.

ACKNOWLEDGMENTS

The authors are indebted to the Computer Centre of the National University of Singapore for expert advice concerning vectorization and speed optimization of the simulation programs for running on the supercomputer. Grateful acknowledgment is also due to Y. Satoh of Tohoku University for his help in collecting some experimental data, and to Wu Tong Meng for technical assistance in the laboratory. This work was supported by National University of Singapore Grant No. RP900651.

[1] G. W. Catlow, M. R. C. McDowell, J. J. Kaufman, L. M. Sachs, and E. S. Chang, J. Phys. B **3**, 833 (1970).
[2] P. C. Harhiharan and V. Staemmler, Chem. Phys. **15**, 409 (1976).
[3] M. Waldman and R. G. Gordon, J. Chem. Phys. **71**, 1325 (1979).
[4] P. Polak-Dingels, M. S. Rajan, and E. A. Gislason, Journal Name **77**, 3983 (1982).
[5] I. R. Gatland, W. F. Morrison, H. W. Ellis, M. G. Thackston, E. W. McDaniel, M. H. Alexander, L. A. Viehland, and E. A. Mason, J. Chem. Phys. **66**, 5121 (1977).
[6] U. E. Senff and P. G. Burton, Mol. Phys. **58**, 637 (1986).
[7] R. Ahlrichs, H. J. Bohm, S. Brode, K. T. Tang, and J. P. Toennies, J. Chem. Phys. **88**, 6290 (1988).
[8] H. R. Skullerud, T. Eide, and Th. Stefansson, J. Phys. D **19**, 197 (1986).
[9] T. H. Lovaas, H. R. Skullerud, O-H. Kirstensen, and D. Linhjell, J. Phys. D **29**, 1465 (1987).
[10] P. H. Larsen, H. R. Skullerud, T. H. Lovaas, and Th. Stefansson J. Phys. B **21**, 2519 (1988).
[11] A. D. Koutselos, E. A. Mason, and L. A. Viehland, J. Chem. Phys. **93**, 7125 (1990).
[12] P. P. Ong and M. J. Hogan, J. Phys. B **24**, 633 (1991).
[13] P. P. Ong and M. J. Hogan, J. Phys. B **24**, 3193 (1991).
[14] M. J. Hogan and P. P. Ong, J. Chem. Phys. **95**, 1973 (1991).
[15] M. J. Hogan and P. P. Ong, Phys. Rev. A **44**, 1597 (1991).
[16] P. P. Ong, M. J. Hogan, K. Y. Lam, and L. A. Viehland, Phys. Rev. A **45**, 3997 (1992).
[17] R. Kubo, Rep. Prog. Phys. **29**, 255 (1966).
[18] E. A. Mason and E. W. McDaniel, *Transport Properties of Ions in Gases* (Wiley, New York, 1988).
[19] M. J. Hogan and P. P. Ong, J. Phys. D **23**, 1050 (1990).
[20] P. P. Ong and M. J. Hogan, Rev. Sci. Instrum. **62**, 1047 (1991).
[21] M. J. Hogan and P. P. Ong, Rev. Sci. Instrum. **61**, 1338 (1990).
[22] A. Cassidy and M. T. Elford, Aust. J. Phys. **38**, 587 (1985).